Bioconjugate Chemistry

pubs.acs.org/bc

Article

Ratiometric Fluorescent Biosensor Based on Self-Assembled Fluorescent Gold Nanoparticles and Duplex-Specific Nuclease-Assisted Signal Amplification for Sensitive Detection of Exosomal miRNA

Zhiwei Sun,[#] Juan Li,[#] Yufei Yang, Yao Tong, Hui Li, Chuanxin Wang, Lutao Du,[*] and Yanyan Jiang[*]

Cite This: *Bioconjugate Chem.* 2022, 33, 1698−1706

Read Online

ACCESS | Metrics & More | Article Recommendations | Supporting Information

ABSTRACT: The sensitive detection of cancer-associated exosomal microRNAs shows enormous potential in cancer diagnosis. Herein, a ratiometric fluorescent biosensor based on self-assembled fluorescent gold nanoparticles (Au NPs) and duplex-specific nuclease (DSN)-assisted signal amplification was fabricated for sensitive detection of colorectal cancer (CRC)-associated exosomal miR-92a-3p. In this biosensing system, the hairpin DNA modified with sulfhydryl and fluorescent dye Atto-425 at both ends is conjugated to fluorescent Au NPs through Au−S bonds, resulting in the quenching of Atto-425. The miR-92a-3p can open the hairpin of DNA and forms an miR-92a-3p/DNA heteroduplex, triggering the specific cleavage of DSN for the DNA in the heteroduplex. As a result, Atto-425 leaves the fluorescent Au NPs and recovers the fluorescence emission. The released miR-92a-3p can hybridize with another hairpin DNA and lead to a stronger fluorescence recovery of Atto-425 to form a signal amplification cycle. The stable fluorescence of Au NPs and the changing fluorescence of Atto-425 constitute a ratiometric fluorescent system reflecting the concentration of miR-92a-3p. This biosensor exhibits excellent specificity and can distinguish CRC patients from healthy individuals by detecting miR-92a-3p extracted from clinical exosome samples, showing the potential in CRC diagnosis.

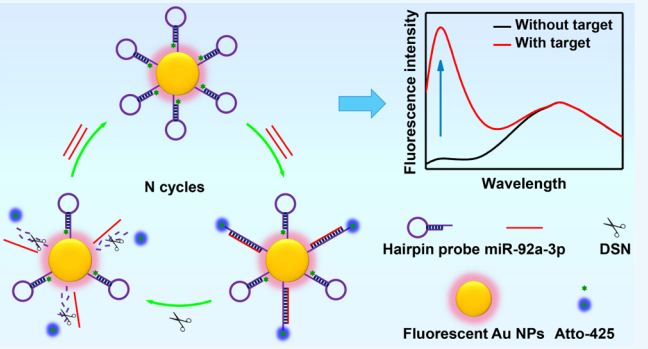

INTRODUCTION

MicroRNAs (miRNAs), a class of single-stranded non-coding RNAs of 18−24 nucleotides, act as regulators of numerous physiological processes by repressing mRNA translation.[1,2] The aberrant expression levels of human miRNAs are related with various pathological situations including cancer.[3,4] Therefore, some specific miRNAs were identified as biomarkers for the diagnosis and prognosis of cancers, and sensitive detection of circulating miRNAs holds great potential in cancer liquid biopsy.[5,6] Exosomes are a subtype of endocytic-derived extracellular vesicles released by almost all cell types.[7] They can be simply described as discoid vesicles composed of a phospholipid bilayer membrane with embedded and linked proteins and internal cargoes including proteins, nucleic acids, lipids, amino acids, and metabolites.[8,9] Exosomes circulate in all body fluids, regulating the composition and behavior of their targets by transporting cargoes to recipient cells.[10] In recent years, the determination of miRNAs in exosomes has received increasing attention because their concentrations in exosomes are higher than those in body fluids, and the expression difference of exosomal miRNAs between healthy individuals and patients is more pronounced.[11−13] In addition, miRNAs in exosomes have been reported to be protected from RNase degradation due to the protection of the phosphate bilayer.[14] Colorectal cancer (CRC) is a major cancer with high morbidity and mortality and is difficult to diagnose in its early stage. Previous research has demonstrated that miR-92a-3p, which is significantly upregulated in CRC patients, is a reliable CRC biomarker.[15] Notably, the level of exosomal miR-92a-3p is highly correlated with the progression of CRC.[16] Thus, it is meaningful to explore the sensitive detection of exosomal miR-92a-3p for the liquid biopsy of CRC.

Reverse transcription-quantitative polymerase chain reaction (RT-qPCR), Northern blotting, and oligonucleotide microarray are conventional methods that have been widely used for the determination of RNAs. Nonetheless, they have some

Received: June 30, 2022
Revised: July 31, 2022
Published: August 12, 2022

https://doi.org/10.1021/acs.bioconjchem.2c00309
Bioconjugate Chem. 2022, 33, 1698−1706

disadvantages such as the need for trained operators (RT-qPCR), expensive equipment (RT-qPCR), complicated procedures (RT-qPCR, Northern blotting, microarray), long analysis time (microarray), low sensitivity (Northern blotting, microarray), and poor reproducibility (microarray).[17,18] The booming next-generation sequencing technology is a high-throughput method that can rapidly sequence base pairs in samples.[19] However, its widespread application is still hampered by the high cost and relatively low accuracy. Therefore, researchers turned to developing novel detection strategies that are sensitive, selective, convenient (without complicated total RNA extraction steps), and easy to operate. These novel strategies are based on various functional nanomaterials and different principles such as fluorescence, surface-enhanced Raman spectroscopy, colorimetry, surface plasmon resonance, electrochemistry, photoelectrochemistry, and electrochemiluminescence.[20−27] Fluorescence-based methods are most commonly used for the determination of miRNAs due to their high sensitivity and simple operation.[28] Various nanomaterials with fluorescence emission or quenching functions such as gold nanoparticles (Au NPs), Ti_3C_2Tx, MoS_2, g-C_3N_4, black phosphorus, graphene oxide, MnO_2 nanosheets, magnetic nanoparticles, metal-organic frameworks, and covalent organic frameworks have been explored for the detection of miRNAs.[29−38] Among them, Au NPs can effectively quench the fluorescence of fluorescent molecules through an energy transfer phenomenon. For instance, Zhao et al. constructed a molecular beacon by attaching Cy5-modified hairpin probes to Au NP-coated polystyrene microbeads.[39] Based on duplex-specific nuclease (DSN)-assisted signal amplification and RGB value measurement, this strategy achieved a detection limit of 50 fM for miRNA-21. In another work, Zhao et al. proposed a thermophoretic sensor implemented with nanoflares for in situ detection of exosomal miRNA.[11] The nanoflare with the target recognition sequence is constructed by functionalizing 13 nm spherical Au NPs with antisense single-stranded DNAs of the target. These DNAs are prehybridized with short DNA sequences modified with Cy5 as reporter flares. The proximity of Cy5 to Au NPs resulted in fluorescence quenching. After the nanoflare is transported into the exosome, the hybridization of DNA probes and target miRNAs makes the reporter flares leave Au NPs to restore the fluorescent signal. The thermophoretic enrichment of nanoflare-loaded exosomes by localized laser heating resulted in fluorescence enhancement caused only by the target miRNAs in exosomes. This strategy can quantitatively detect exosomal miRNAs as low as 0.36 fM in 0.5 μL of serum samples. However, the strategy based on measuring absolute changes in fluorescence intensity is susceptible to interference by some experimental conditions such as light source stability and solution thermodynamic fluctuations.[40] Comparatively, ratiometric fluorometry is capable of self-referencing by calculating the ratio of fluorescence intensities at two different wavelengths to eliminate the effects of environmental conditions.[41] Thus, it is a reliable strategy to construct a ratiometric fluorescent biosensor for miRNA detection.

Sensitive detection of miRNAs remains difficult because of their low expression and high sequence similarity.[42] Therefore, some signal amplification strategies such as nicking enzyme-assisted amplification, DSN-assisted amplification, rolling circle amplification, catalytic hairpin assembly, and hybridization chain reaction have been introduced to improve the sensitivity.[43−48] Among them, DSN-based miRNA biosensing is regarded as a promising strategy with the merits of high sensitivity and specificity. DSN can cleave the DNA strand in an RNA−DNA heteroduplex with more than 10−12 consecutive complementary nucleotides into DNA fragments while keeping the RNA strand intact.[49] The complete target miRNA can be reused to form a new heteroduplex for the next step of cleavage. In the current work, we fabricated a ratiometric fluorescent biosensor based on fluorescent Au NPs and DSN-assisted signal amplification for the detection of exosomal miR-92a-3p. Au NPs were synthesized by the self-assembly of gold nanoclusters (Au NCs), which performed dual functions of a fluorescence quencher and an internal fluorescence reference standard. Fluorescent dye Atto-425- and thiol-modified hairpin DNA was conjugated to fluorescent Au NPs through a Au−S bond to form a nanoprobe. The target miR-92a-3p in the sample can open the hairpin of DNA to form an RNA−DNA heteroduplex. This triggers the specific cleavage of the DNA in the RNA−DNA heteroduplex by DSN and the departure of Atto-425 from the surface of fluorescent Au NPs. The fluorescence of Atto-425 is thus recovered, and the miR-92a-3p is released. The released miR-92a-3p can bind to other hairpin DNA to form a cycle. The concentration of miR-92a-3p can be calculated according to the ratio of fluorescence intensities of Atto-425 and fluorescent Au NPs. Specifically, we first characterized the physicochemical properties of Au NCs and fluorescent Au NPs. Then, the feasibility of nucleic acid reaction and ratiometric fluorescent detection was demonstrated by non-denaturing polyacrylamide gel electrophoresis and fluorescence measurements. Subsequently, we optimized the experimental conditions and explored the sensitivity and specificity of the detection. Finally, the practicality of the proposed biosensor was verified by detecting the concentrations of exosomal miR-92a-3p extracted from clinical serum samples.

RESULTS AND DISCUSSION

Properties of Au NCs and Fluorescent Au NPs. Au NCs were synthesized by reduction of $HAuCl_4$ with glutathione (GSH) under a nitrogen atmosphere. As shown in Figure 1a, the size of Au NCs is uniform with a distribution range of 2.1−3.7 nm. The electron diffraction pattern shows diffraction rings attributed to the (111), (220), and (311) planes of Au, which demonstrates that the Au NCs are successfully synthesized (Figure 1b). The Au NCs stabilized by ethanol-insoluble GSH can aggregate into Au NPs upon the addition of ethanol. Therefore, fluorescent Au NPs were synthesized by the self-assembly of Au NCs induced by ethanol. As shown in Figure 1c, the size range of fluorescent Au NPs is 42−85 nm. The electron diffraction pattern in Figure 1d indicates that the self-assembled product is Au NPs without other impurities. In addition, the microstructure of fluorescent Au NPs was further observed by high-resolution transmission electron microscopy (HRTEM). As shown in Figure S1, the fluorescent Au NPs appear as aggregates of Au NCs, which proves that the fluorescent Au NPs are formed by the self-assembly of Au NCs.

As shown in Figure 2a, the zeta potential of Au NCs is −4.6 mV while that of fluorescent Au NPs is −11.9 mV. This indicates that the dispersion of fluorescent Au NPs in water is better than that of Au NCs. The increased negative zeta potential of fluorescent Au NPs compared to Au NCs may be attributed to the increase in carboxyl groups on the surface of individual particles. The fluorescence excitation and emission

https://doi.org/10.1021/acs.bioconjchem.2c00309
Bioconjugate Chem. 2022, 33, 1698−1706

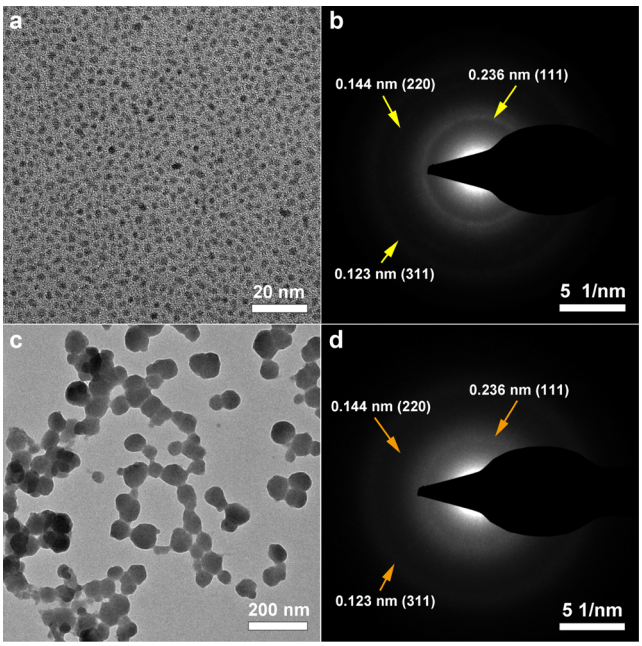

Figure 1. (a) TEM image and (b) electron diffraction pattern of Au NCs. (c) TEM image and (d) electron diffraction pattern of fluorescent Au NPs.

spectra of Au NPs were measured, as shown in Figure 2b. The fluorescence emission peak of Au NPs is located at 625 nm, and the fluorescence intensity increases with the decreasing excitation wavelength. This may be attributed to the fact that the short-wavelength excitation light with higher energy can excite more electronic transitions. The UV−vis absorption spectra of Au NCs and fluorescent Au NPs were also measured (Figure 2c). The absorbance of Au NCs decreases with the increasing irradiation wavelength, which is consistent with the trend of the plasmon resonance effect. The broad weak absorption peak around 410 nm of the fluorescent Au NPs corresponds to its broad size distribution. The emission stability under continuous excitation is an important indicator to evaluate the practicality of the fluorescent materials. As shown in Figure 2d, the fluorescence intensities of Au NCs and Au NPs maintain 81.3 and 91.7% of the initial values after 10 min irradiation, respectively. Obviously, the fluorescence emission stability of fluorescent Au NPs is better than that of Au NCs. This is attributed to the formation of dense and rigid self-assembled aggregates under a hydrophobic effect. The robust internal interaction suppresses particle vibration, thus emitting stable fluorescence.[50] In addition, the larger negative surface charge of the fluorescent Au NPs might suppress the particle collision-induced quenching.

Principle of Detection. The principle of ratiometric fluorescent detection of miR-92a-3p is depicted in Scheme 1. Hairpin DNA is modified with Atto-425 at the 5′ end and sulfhydryl at the 3′ end, followed by conjugation with the fluorescent Au NPs via a Au−S bond.[51] The fluorescence excitation and emission spectra of Atto-425 are presented in Figure S2. The excitation spectrum of Atto-425 shows two peaks at 320 and 443 nm. The fluorescence emission peak of Atto-425 is located at 482 nm. The fluorescence of Atto-425 is quenched by the fluorescent Au NPs due to the proximity. In the presence of miR-92a-3p, the hairpin of DNA is opened, and an RNA−DNA heteroduplex is formed. The fluorescence of Atto-425 is recovered as it leaves the surface of fluorescent Au NPs. The formation of the RNA−DNA heteroduplex triggers the cleavage of DNA by DSN and the release of miR-92a-3p and Atto-425. The released miR-92a-3p can hybridize with other hairpin DNA to form a cycle, resulting in a significant fluorescence recovery of Atto-425. The ratiometric fluorescent system composed of changing cyan fluorescence of Atto-425 and stable red fluorescence of Au NPs indicates the concentration of miR-92a-3p. The concentration of hairpin DNA in the nanoprobe (fluorescent Au NPs conjugated with

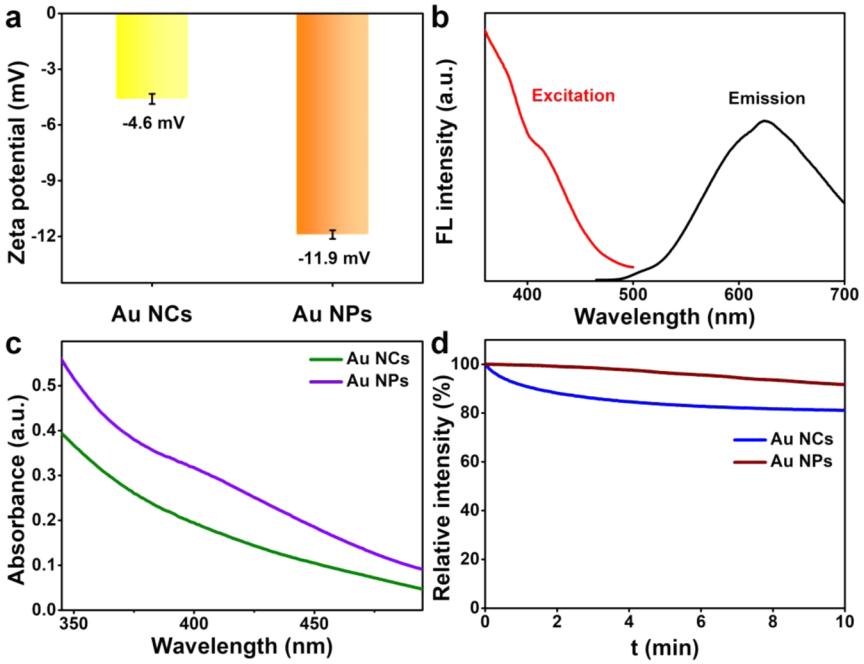

Figure 2. (a) Zeta potentials of Au NCs and fluorescent Au NPs. (b) Fluorescence excitation and emission spectra of Au NPs. (c) UV−vis absorption spectra of Au NCs and fluorescent Au NPs. (d) Fluorescence stability of Au NCs and fluorescent Au NPs under continuous irradiation.

https://doi.org/10.1021/acs.bioconjchem.2c00309
Bioconjugate Chem. 2022, 33, 1698−1706

Scheme 1. Schematic of the Ratiometric Fluorescent Detection of miR-92a-3p Based on Fluorescent Au NPs and DSN-Assisted Signal Amplification

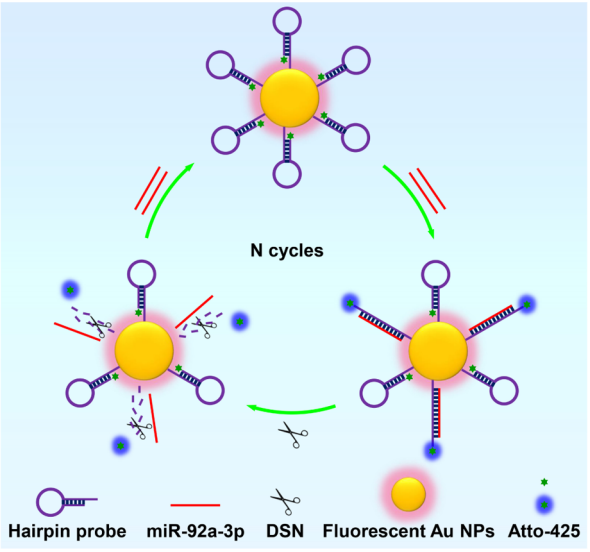

hairpin DNA) was calculated using a UV−vis absorption spectrum. As shown in Figure S3, a standard curve is drawn by the absorbance of the nanoprobe solution at 260 nm and the concentration of hairpin DNA. According to the fitting equation in Figure S3b and absorbance, the hairpin DNA concentration of the prepared nanoprobe solution was calculated to be 0.96 μM, which means that 96% of the hairpin DNA is connected to the fluorescent Au NPs through Au−S bonds.

Non-denaturing polyacrylamide gel electrophoresis of different oligonucleotide systems was performed to verify the feasibility of the nucleic acid reaction. As shown in Figure 3a, the electrophoresis speed of miR-92a-3p+hairpin DNA is lower than that of miR-92a-3p and hairpin DNA, demonstrating that miR-92a-3p can open the hairpin of DNA and form an RNA−DNA heteroduplex. In the presence of DSN, the electrophoresis speed of the miR-92a-3p+hairpin DNA band is accelerated, indicating that the RNA−DNA heteroduplex is cleaved by DSN. The feasibility of the ratiometric fluorescent detection was verified by fluorescence measurements (Figure 3b). In the system composed of hairpin DNA and fluorescent Au NPs, the fluorescence intensity of Atto-425 is significantly reduced, indicating that the fluorescent Au NPs can effectively quench the fluorescence of Atto-425. The presence of miR-92a-3p (3 pM) results in a weak recovery of the fluorescence of Atto-425, implying the formation of the RNA−DNA heteroduplex. The addition of DSN results in a significant recovery of the Atto-425 fluorescence, demonstrating the feasibility of the DSN-assisted signal amplification strategy. In short, non-denaturing polyacrylamide gel electrophoresis and fluorescence measurements demonstrate that the proposed ratiometric fluorescence biosensor is feasible for miR-92a-3p detection.

Optimization of the Experimental Conditions. Prior to the detection of miR-92a-3p, the experimental conditions including reaction time between hairpin DNA and fluorescent Au NPs, the amount of DSN used in the incubation, incubation temperature, and time of the detection process were optimized. To determine the time required for the stable connection between hairpin DNA and fluorescent Au NPs, the fluorescence intensities of Atto-425 at different mixing times were measured. The fluorescence intensity of Atto-425 decreases with the increasing reaction time (Figure 4a). When the reaction time increases from 10 to 12 h, the decrease in the fluorescence intensity of Atto-425 is significantly reduced, and the fluorescence intensity of Atto-425 is approximately 15% of the initial value. Thus, 12 h is determined as the optimal reaction time. The amount of DSN can significantly affect the efficiency of the amplification reaction. Therefore, the fluorescence signals of the detection system were measured under different DSN dosages from 0.01 to 0.2 U. An miR-92a-3p concentration of 5 pM and an incubation time of 2 h were set. It can be observed from Figure 4b that the reaction efficiency increases with the increasing DSN. The fluorescence signals tend to be stable when the amount of DSN adds up to ∼0.09 U, and more DSN cannot lead to a significant change of the signal. To ensure the high efficiency of DSN-assisted signal amplification, the DSN dosage in subsequent experiments is determined to be 0.2 U. The incubation temperature can significantly affect the activity of DSN. Hence, the influence of incubation temperature on the fluorescence signals of the detection system under an miR-92a-3p concentration of 2 pM and an incubation time of 2 h was investigated. As displayed in Figure 4c, the maximum $(F - F_0)_{482}/F_{625}$ value is obtained at 45 °C, while a lower or higher

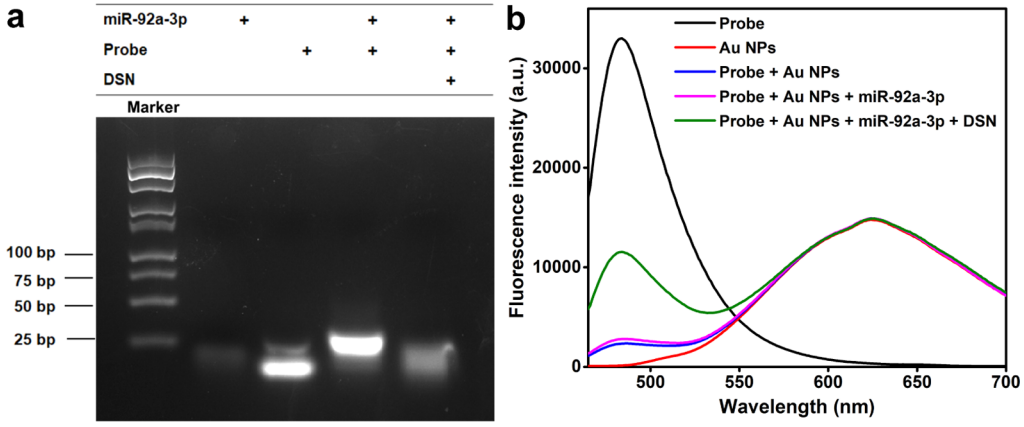

Figure 3. (a) Non-denaturing polyacrylamide gel electrophoresis image. (b) Fluorescence spectra of hairpin DNA, fluorescent Au NPs, hairpin DNA + fluorescent Au NPs, hairpin DNA + fluorescent Au NPs + miR-92a-3p, and hairpin DNA + fluorescent Au NPs + miR-92a-3p + DSN.

https://doi.org/10.1021/acs.bioconjchem.2c00309
Bioconjugate Chem. 2022, 33, 1698−1706

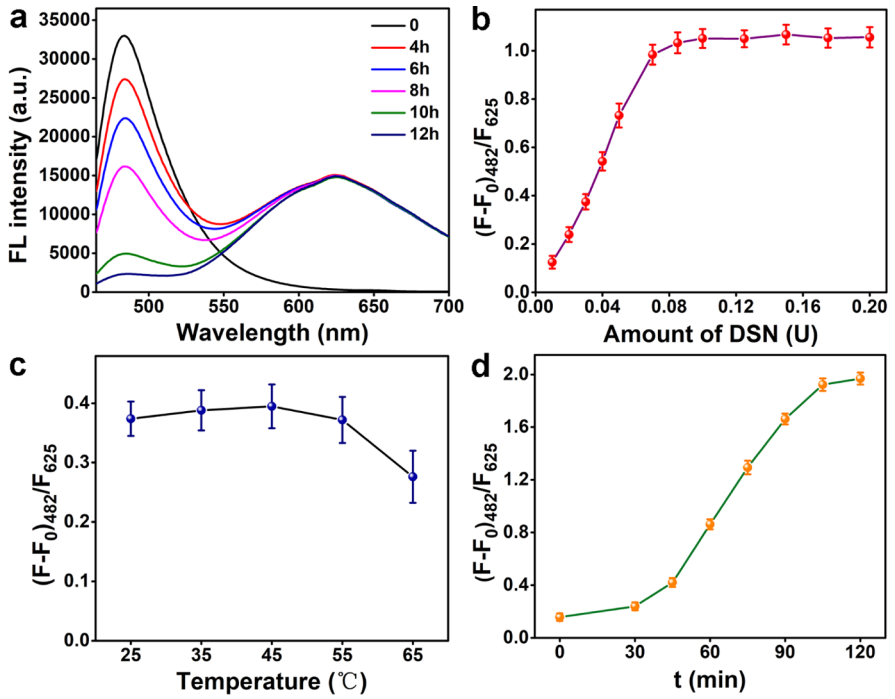

Figure 4. (a) Effect of the reaction time between hairpin DNA and fluorescent Au NPs on the fluorescence intensity of Atto-425. Effect of the (b) amount of DSN, (c) incubation temperature, and (d) incubation time on the fluorescence signal (n = 3, mean ± s.d.).

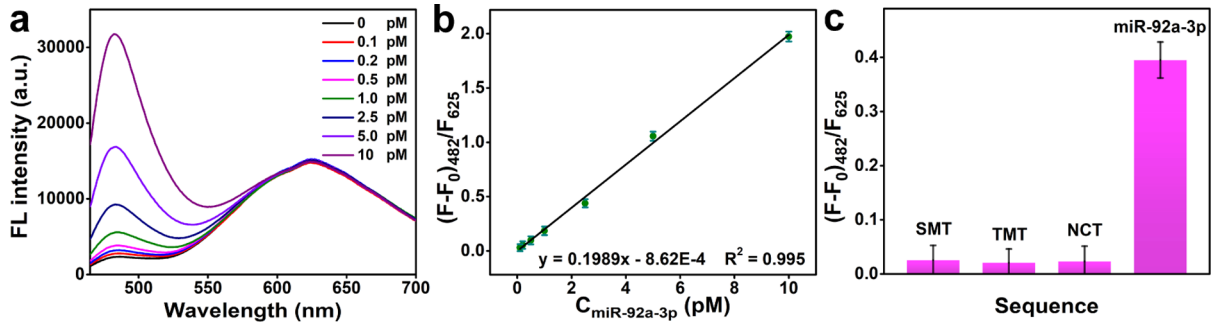

Figure 5. (a) Fluorescence spectra of the biosensor under different concentrations of miR-92a-3p. (b) Calibration line of the fluorescence signals against the concentration of miR-92a-3p. (c) Comparison of the fluorescence signals produced by miR-92a-3p and mismatched sequences (n = 3, mean ± s.d.).

temperature results in the decreased $(F - F_0)_{482}/F_{625}$ value due to the inefficient hybridization between hairpin DNA and miR-92a-3p or the reduction of the activity of DSN. Thus, 45 °C is determined to be the optimal incubation temperature. The optimal incubation time for the detection was explored under an miR-92a-3p concentration of 10 pM (Figure 4d). On incubation within 45 min, the value of $(F - F_0)_{482}/F_{625}$ increases slowly. The value of $(F - F_0)_{482}/F_{625}$ increases rapidly at 45−105 min, indicating that the nucleic acid reaction and enzymatic reaction proceed rapidly in this interval. A slight increase in the $(F - F_0)_{482}/F_{625}$ value is observed at 105−120 min, indicating that the reaction is almost completed in 120 min. Therefore, 120 min is determined to be the optimal incubation time.

Sensitivity and Selectivity for miR-92a-3p Detection. The sensitivity of the proposed biosensor for miR-92a-3p detection was measured under optimized experimental conditions. It can be seen from Figure 5a,b that the fluorescence intensities of Atto-425 linearly increase with the concentration of miR-92a-3p from 0.1 to 10 pM. A calculated detection limit of 45 fM is obtained according to the 3σ method. The goodness of fit of the regression equation is 0.995, indicating that the biosensor shows excellent regularity and stability. Compared to previously reported ratiometric fluorescent biosensors shown in Table 1, our fabricated biosensor shows a satisfactory linear interval and detection limit, demonstrating its potential for sensitive miRNA detection. To evaluate the selectivity of the proposed biosensor, the concentration determinations were performed with a single-base mismatched target (SMT), two base-mismatched target (TMT), and non-complementary target (NCT) as control sequences. The preset concentration of all oligonucleotides is 2 pM, and the corresponding fluorescence signals are shown in Figure 5c. The $(F - F_0)_{482}/F_{625}$ values corresponding to three mismatched sequences are significantly lower than those of miR-92a-3p, indicating that the mismatched sequences cannot cause noticeable fluorescence recovery of Atto-425. According to the regression equation, the measured concentrations of the SMT, TMT, and NCT are 0.14, 0.11, and 0.12 pM, respectively, which are much lower

https://doi.org/10.1021/acs.bioconjchem.2c00309
Bioconjugate Chem. 2022, 33, 1698−1706

Table 1. Comparison of the Detection Performance of the Ratiometric Fluorescent Biosensors for miRNAs

fluorescent materials	targets	linear interval (pM)	limit of detection (pM)	ref
protonated phenyl-doped carbon nitride, ROX	miRNA-224	10^3–2×10^4	200	52
FAM, TAMRA	miRNA-21	10^2–2×10^4	73	53
NMM, DAPI	miRNA-21	10–4.5×10^4	3.1	41
CDs, FAM	miRNA-21	5×10^1–1×10^4	1	54
CdTe QDs, FCMMs	let-7a	2–2×10^2	0.1	55
boron-doped g-C_3N_4 nanosheets, Cu NCs	miR-582-3p	0.2–1	0.049	32
fluorescent Au NPs, Atto-425	miR-92a-3p	0.1–10	0.045	this work

than their real concentrations. This indicates that the proposed biosensor has good selectivity.

Detection of miR-92a-3p Extracted from Exosomes. Before measuring the concentration of exosomal miR-92a-3p, exosomes were extracted from human sera, and the exosomal miR-92a-3p was obtained by lysing the exosomes. First, the morphology of the exosomes was characterized by TEM. As shown in Figure 6a, exosomes are spherical and exhibit dimensions in the range of 27–115 nm. According to the literature, exosomes may shrink during TEM sample preparation, which results in the observed size of exosomes being smaller than their actual size.[56] Furthermore, exosomes were identified by western blotting. The marker proteins of exosomes, TSG101 and CD9, were detected. Exosome-enriched and exosome-unenriched serum samples from one CRC patient and one healthy individual were used for the assay. As seen from Figure 6b, the western blotting images demonstrate that there are abundant TSG101 and CD9 in the exosome-enriched samples. The significant binding validates the efficient extraction of exosomes.

To evaluate the practicality of the detection, RT-qPCR and the ratiometric fluorescent biosensor were used in parallel to determine exosomal miR-92a-3p extracted from six CRC patients and six healthy controls. The real-time fluorescence curves of miR-92a-3p at different preset concentrations measured by RT-qPCR are shown in Figure S4. A fitted standard curve was obtained based on the cycle values at ΔR_n of 1×10^5 in the real-time fluorescence curves (Figure S5). As shown in Figure 6c, the concentrations of exosomal miR-92a-3p extracted from clinical serum samples detected using the ratiometric fluorescent biosensor are well consistent with those of RT-qPCR, demonstrating that our fabricated biosensor possesses satisfactory accuracy and practicality. In addition, because of the flexible sequence modification of the nanoprobe, other RNAs can also be detected using this biosensor via simply changing the sequence of the nanoprobe.

CONCLUSIONS

In summary, we fabricated a ratiometric fluorescent biosensor for the sensitive detection of exosomal miR-92a-3p, a biomarker of CRC. The nanoprobe is composed of fluorescent Au NPs and hairpin DNA conjugated with the fluorescent Au NPs. The fluorescence of Atto-425 modified on the hairpin DNA is quenched by the fluorescent AuNPs. The presence of the miR-92a-3p results in the departure of Atto-425 from the surface of fluorescent Au NPs and the recovery of the fluorescence of Atto-425. A large amount of Atto-425 leaves the surface of fluorescent Au NPs under the action of DSN, resulting in a significant amplification of the fluorescence signal. The concentration of miR-92a-3p can be calculated based on the fluorescence intensities of Atto-425 and fluorescent Au NPs. A detection concentration interval of 0.1–10 pM and a detection limit of 45 fM are obtained under the optimized experimental conditions. This biosensor can differentiate miR-92a-3p from mismatched sequences and can accurately detect the concentration of miR-92a-3p extracted from exosomes, showing its potential for clinical diagnosis.

MATERIALS AND METHODS

Samples and Materials. All serum samples were obtained from healthy controls and CRC patients at the Second Hospital of Shandong University. This work was approved by the ethics committee of the Second Hospital of Shandong University [project number: KYLL-2019(KJ)P-0067].

Tetrachloroauric(III) acid tetrahydrate ($HAuCl_4 \cdot 4H_2O$, AR grade), glutathione reduced (GSH; $C_{10}H_{17}N_3O_6S$, ≥98%), tris(2-carboxyethyl)phosphine hydrochloride (TCEP; $C_9H_{15}O_6P \cdot HCl$, 98%), and ethanol absolute (C_2H_6O, ≥99.8%) were purchased from Sinopharm Chemical Reagent Co., Ltd. DSN (1 U/μL) was purchased from Evrogen JSC. Atto-425- and sulfhydryl-modified hairpin DNA was purchased from Sangon Biotech (Shanghai) Co., Ltd. miR-92a-3p and mismatched sequences were purchased from Shanghai Genepharma Co., Ltd. Ultrapure water was used in all

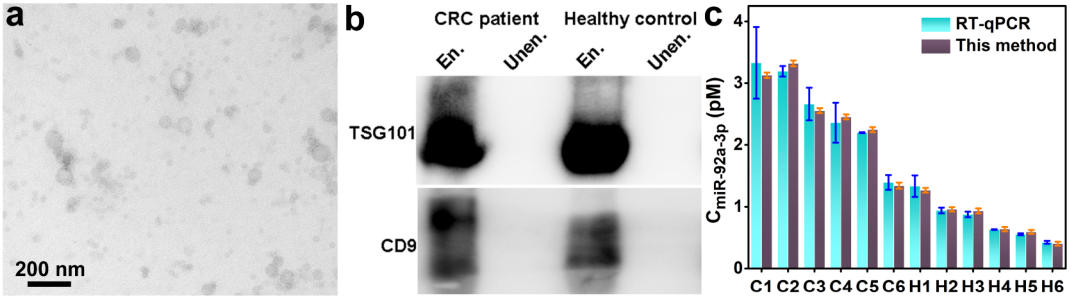

Figure 6. (a) TEM image of exosomes. (b) Comparison of the western blotting of exosome-enriched (En.) sera and exosome-unenriched (Unen.) sera. (c) Comparison of the exosomal miR-92a-3p concentrations of CRC patients and healthy controls detected by RT-qPCR and this method (n = 3, mean ± s.d.). C1–C6 represent CRC patients; H1–H6 represent healthy controls.

https://doi.org/10.1021/acs.bioconjchem.2c00309
Bioconjugate Chem. 2022, 33, 1698–1706

experiments. All oligonucleotide sequences are listed in Table 2.

Table 2. Oligonucleotide Sequences Used in This Work

oligonucleotide	sequence (5′ → 3′)
hairpin DNA	Atto-425-ACTTGTACAGGCCGGGACAAGTGCAATATT-SH
miR-92a-3p	UAUUGCACUUGUCCCGGCCUGU
SMT	UAUUCCACUUGUCCCGGCCUGU
TMT	UUUUCCACUUGUCCCGGCCUGU
NCT	UGUCAGUUUGUCAAAUACCCCA

Synthesis of Au NCs and Fluorescent Au NPs. *Synthesis of Au NCs.* 10 mL of $HAuCl_4{\cdot}4H_2O$ aqueous solution (4 mM) was added to a three-necked flask and stirred at 25 °C for 5 min under a nitrogen atmosphere. Then, 10 mL of $C_{10}H_{17}N_3O_6S$ aqueous solution (6 mM) was injected and stirred for 10 min. Subsequently, the solution was refluxed at 100 °C for 12 h. After naturally cooling to room temperature, the purified Au NC aqueous solution was obtained by dialyzing six times with ultrapure water for 24 h.

Synthesis of Fluorescent Au NPs by Self-Assembly of Au NCs. Ethanol was added dropwise into Au NC aqueous solution at a Au NC aqueous solution/ethanol volume ratio of 4:1 and stirred vigorously at 25 °C for 2 h. The purified fluorescent Au NP aqueous solution was obtained by dialyzing six times with ultrapure water for 24 h. The process of synthesizing fluorescent Au NPs is depicted in Scheme 2.

Conjugation of Hairpin DNA on Fluorescent Au NPs. First, the sulfhydryl of the hairpin DNA was activated by TCEP through mixing equal volumes of hairpin DNA aqueous solution (10 μM) and TCEP aqueous solution (1 mM) for 1 h. Then, hairpin DNA aqueous solution (5 μL, 2 μM), fluorescent Au NP aqueous solution (90 μL), and NaCl aqueous solution (5 μL, 1 M) were mixed and reacted at 4 °C for 12 h. Finally, the product solution was purified by dialysis six times with ultrapure water for 24 h.

Ratiometric Fluorescent Detection of miR-92a-3p. First, nanoprobe aqueous solution (100 μL), the target (5 μL) with different concentrations, DSN (0.2 U), and DSN master buffer (10 μL) were mixed and incubated at 45 °C for 2 h. Then, 5 μL of DSN stop solution (10 mM EDTA) was dropped and kept for 10 min to inactivate DSN. The total volume of the solution was quantified to 2 mL by adding ultrapure water. Finally, the signals were collected using a fluorescence spectrophotometer. The excitation wavelength was 430 nm, and the slits of excitation and emission were both 15 nm. The emission spectra in the range of 465−700 nm were collected. For clinical sample detection, only replacing the target with the same volume of extracted exosomal RNAs is needed. All measurements were parallelly performed three times, and the averages were reported.

Additional Experiments. The details of apparatus used, extraction of exosomes and exosomal RNAs, and RT-qPCR detection of miR-92a-3p are described in the Supporting Information.

■ ASSOCIATED CONTENT

Supporting Information

The Supporting Information is available free of charge at https://pubs.acs.org/doi/10.1021/acs.bioconjchem.2c00309.

Apparatus for characterization, HRTEM images of fluorescent Au NPs, fluorescence spectra of Atto-425, UV−vis absorption spectra of solutions consisting of fluorescent Au NPs and hairpin DNA with different concentrations, calibration line of the hairpin DNA concentration against absorbance, RT-qPCR curves corresponding to different concentrations of miR-92a-3p, and calibration line of Ct against the concentration of miR-92a-3p (PDF)

■ AUTHOR INFORMATION

Corresponding Authors

Lutao Du − *Department of Clinical Laboratory, The Second Hospital of Shandong University, Jinan 250033, China*; Email: lutaodu@sdu.edu.cn

Yanyan Jiang − *Key Laboratory for Liquid−Solid Structural Evolution and Processing of Materials, Ministry of Education, Shandong University, Jinan 250061, China; Shenzhen Research Institute of Shandong University, Shenzhen 518057, China*; orcid.org/0000-0002-7866-4689; Email: yanyan.jiang@sdu.edu.cn

Authors

Zhiwei Sun − *Key Laboratory for Liquid−Solid Structural Evolution and Processing of Materials, Ministry of Education, Shandong University, Jinan 250061, China; Shenzhen Research Institute of Shandong University, Shenzhen 518057, China*

Scheme 2. Schematic of the Process of Synthesizing Fluorescent Au NPs

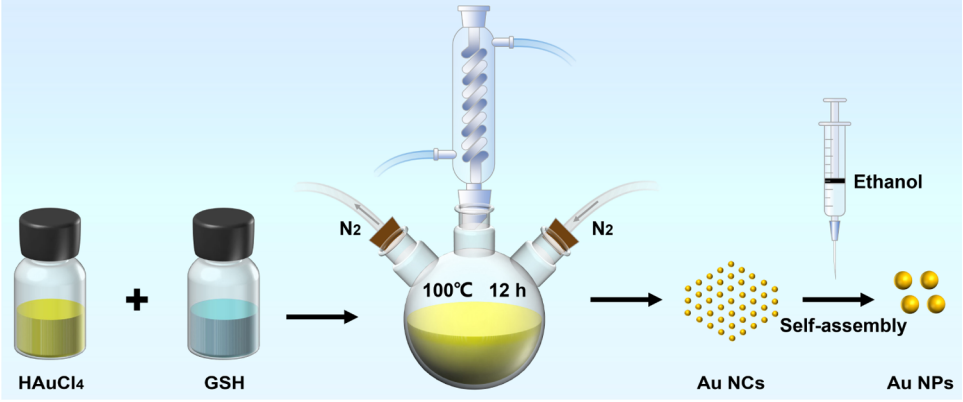

https://doi.org/10.1021/acs.bioconjchem.2c00309
Bioconjugate Chem. 2022, 33, 1698−1706

Juan Li − *Department of Clinical Laboratory, The Second Hospital of Shandong University, Jinan 250033, China*
Yufei Yang − *Key Laboratory for Liquid−Solid Structural Evolution and Processing of Materials, Ministry of Education, Shandong University, Jinan 250061, China*
Yao Tong − *Department of Clinical Laboratory, The Second Hospital of Shandong University, Jinan 250033, China*
Hui Li − *Key Laboratory for Liquid−Solid Structural Evolution and Processing of Materials, Ministry of Education, Shandong University, Jinan 250061, China;* orcid.org/0000-0002-1457-8650
Chuanxin Wang − *Department of Clinical Laboratory, The Second Hospital of Shandong University, Jinan 250033, China; Shandong Engineering & Technology Research Center for Tumor Marker Detection, Jinan 250033, China; Shandong Provincial Clinical Medicine Research Center for Clinical Laboratory, Jinan 250033, China;* orcid.org/0000-0002-3796-6293

Complete contact information is available at: https://pubs.acs.org/10.1021/acs.bioconjchem.2c00309

Author Contributions

[#]Z.S. and J.L. contributed equally to this work.

Notes

The authors declare no competing financial interest.

■ ACKNOWLEDGMENTS

This work was financially supported by the National Natural Science Foundation of China (grant nos. 52101287 and U1806219), the Shenzhen Fundamental Research Program (grant no. JCYJ20190807092803583), the Natural Science Foundation of Jiangsu Province (grant no. BK20190205), and the Basic and Applied Basic Research Foundation of Guangdong Province (grant no. 2019A1515110846). This work was also supported by the special fund of the Project of the Qilu Young Scholar Program of Shandong University.

■ REFERENCES

(1) Abu-Izneid, T.; AlHajri, N.; Ibrahim, A. M.; Javed, M. N.; Salem, K. M.; Pottoo, F. H.; Kamal, M. A. Micro-RNAs in the regulation of immune response against SARS CoV-2 and other viral infections. *J. Adv. Res.* **2021**, *30*, 133−145.
(2) Kobayashi, H.; Singer, R. H. Single-molecule imaging of microRNA-mediated gene silencing in cells. *Nat. Commun.* **2022**, *13*, 1435.
(3) Ji, C. M.; Gao, Z.; Ma, X.; Wu, Q. W.; Ni, J. C.; Zheng, C. H. AEMDA: inferring miRNA-disease associations based on deep autoencoder. *Bioinformatics* **2021**, *37*, 66−72.
(4) Ali Syeda, Z.; Langden, S. S. S.; Munkhzul, C.; Lee, M.; Song, S. J. Regulatory Mechanism of MicroRNA Expression in Cancer. *Int. J. Mol. Sci.* **2020**, *21*, 1723.
(5) Wu, Y.; Zhang, Y.; Zhang, X. H.; Luo, S. H.; Yan, X. H.; Qiu, Y. R.; Zheng, L.; Li, L. Research advances for exosomal miRNAs detection in biosensing: From the massive study to the individual study. *Biosens. Bioelectron.* **2021**, *177*, 112962.
(6) Sohel, M. M. H. Circulating microRNAs as biomarkers in cancer diagnosis. *Life Sci.* **2020**, *248*, 117473.
(7) Sun, Z. W.; Yang, J. J.; Li, H.; Wang, C. X.; Fletcher, C.; Li, J.; Zhan, Y.; Du, L. T.; Wang, F. L.; Jiang, Y. Y. Progress in the research of nanomaterial-based exosome bioanalysis and exosome-based nanomaterials tumor therapy. *Biomaterials* **2021**, *274*, 120873.
(8) Kalluri, R.; LeBleu, V. S. The biology, function, and biomedical applications of exosomes. *Science* **2020**, *367*, No. eaau6977.
(9) Huang, T.; Deng, C. X. Current Progresses of Exosomes as Cancer Diagnostic and Prognostic Biomarkers. *Int. J. Biol. Sci.* **2019**, *15*, 1−11.
(10) Xiong, H. W.; Huang, Z. P.; Yang, Z.; Lin, Q. Y.; Yang, B.; Fang, X. E.; Liu, B. H.; Chen, H.; Kong, J. L. Recent Progress in Detection and Profiling of Cancer Cell-Derived Exosomes. *Small* **2021**, *17*, 2007971.
(11) Zhao, J. X.; Liu, C.; Li, Y. K.; Ma, Y.; Deng, J. Q.; Li, L. L.; Sun, J. Thermophoretic Detection of Exosomal microRNAs by Nanoflares. *J. Am. Chem. Soc.* **2020**, *142*, 4996−5001.
(12) Zhang, R. Y.; Luo, S. H.; Lin, X. M.; Hu, X. M.; Zhang, Y.; Zhang, X. H.; Wu, C. M.; Zheng, L.; Wang, Q. A novel electrochemical biosensor for exosomal microRNA-181 detection based on a catalytic hairpin assembly circuit. *Anal. Chim. Acta* **2021**, *1157*, 338396.
(13) Sun, Z. W.; Tong, Y.; Zhao, L.; Li, J.; Gao, F. C.; Wang, C. X.; Li, H.; Du, L. T.; Jiang, Y. Y. MoS2@Ti3C2 nanohybrid-based photoelectrochemical biosensor: A platform for ultrasensitive detection of cancer biomarker exosomal miRNA. *Talanta* **2022**, *238*, 123077.
(14) Xia, Y. K.; Wang, L. L.; Li, J.; Chen, X. Q.; Lan, J. M.; Yan, A.; Lei, Y.; Yang, S.; Yang, H. H.; Chen, J. H. A Ratiometric Fluorescent Bioprobe Based on Carbon Dots and Acridone Derivate for Signal Amplification Detection Exosomal microRNA. *Anal. Chem.* **2018**, *90*, 8969−8976.
(15) Ahmadi, S.; Sharifi, M.; Salehi, R. Locked nucleic acid inhibits miR-92a-3p in human colorectal cancer, induces apoptosis and inhibits cell proliferation. *Cancer Gene Ther.* **2016**, *23*, 199−205.
(16) Hu, J. L.; Wang, W.; Lan, X. L.; Zeng, Z. C.; Liang, Y. S.; Yan, Y. R.; Song, F. Y.; Wang, F. F.; Zhu, X. H.; Liao, W. J.; et al. CAFs secreted exosomes promote metastasis and chemotherapy resistance by enhancing cell stemness and epithelial-mesenchymal transition in colorectal cancer. *Mol. Cancer* **2019**, *18*, 91.
(17) Gao, X. H.; Li, S.; Ding, F.; Fan, H. J.; Shi, L. L.; Zhu, L. J.; Li, J.; Feng, J.; Zhu, X. Y. .; Zhang, C. Rapid Detection of Exosomal MicroRNAs Using Virus-Mimicking Fusogenic Vesicles. *Angew. Chem., Int. Ed.* **2019**, *58*, 8719−8723.
(18) Fang, C. X.; Ouyang, P.; Yang, Y. X.; Qing, Y.; Han, J. L.; Shang, W. Y.; Chen, Y. B.; Du, J. MiRNA Detection Using a Rolling Circle Amplification and RNA-Cutting Allosteric Deoxyribozyme Dual Signal Amplification Strategy. *Biosensors* **2021**, *11*, 222.
(19) Lu, D. C.; Thum, T. RNA-based diagnostic and therapeutic strategies for cardiovascular disease. *Nat. Rev. Cardiol.* **2019**, *16*, 661−674.
(20) Hu, O.; Li, Z. Y.; Tong, Y. L.; Wang, Q. Y.; Chen, Z. G. DNA functionalized double quantum dots-based fluorescence biosensor for one-step simultaneous detection of multiple microRNAs. *Talanta* **2021**, *235*, 122763.
(21) Meng, X.; Qiu, L.; Xi, G.; Wang, X.; Guo, L. Smart design of high-performance surface-enhanced Raman scattering substrates. *SmartMat.* **2021**, *2*, 466−487.
(22) Kim, J.; Park, J.; Ki, J.; Rho, H. W.; Huh, Y. M.; Kim, E.; Son, H. Y.; Haam, S. Simultaneous dual-targeted monitoring of breast cancer circulating miRNA via surface-enhanced Raman spectroscopy. *Biosens. Bioelectron.* **2022**, *207*, 114143.
(23) Wei, X. T.; Liu, D. W.; Zhao, M.; Yang, T. T.; Fan, Y. P.; Chen, W. Q.; Liu, P.; Li, J. B.; Ding, S. J. An enzyme-free surface plasmon resonance imaging biosensing method for highly sensitive detection of microRNA based on catalytic hairpin assembly and spherical nucleic acid. *Anal. Chim. Acta* **2020**, *1108*, 21−27.
(24) Guo, Q. S.; Bian, F. K.; Liu, Y. Q.; Qu, X. J.; Hu, X. Y.; Sun, Q. J. Hybridization chain reactions on silica coated Qbeads for the colorimetric detection of multiplex microRNAs. *Chem. Commun.* **2017**, *53*, 4954−4957.
(25) Xu, E. S.; Feng, Y. H.; Yang, H. T.; Li, P.; Kong, L.; Wei, W.; Liu, S. Q. Ultrasensitive and specific multi-miRNA detection based on dual signal amplification. *Sens. Actuators, B* **2021**, *337*, 129745.
(26) Song, W. L.; Zhang, F.; Song, P.; Zhang, Z. H.; He, P.; Li, Y.; Zhang, X. R. Untrasensitive photoelectrochemical sensor for micro-

RNA detection with DNA walker amplification and cation exchange reaction. *Sens. Actuators, B* **2021**, *327*, 128900.
(27) Kerr, E.; Farr, R.; Doeven, E. H.; Nai, Y. H.; Alexander, R.; Guijt, R. M.; Prieto-Simon, B.; Francis, P. S.; Dearnley, M.; Hayne, D. J.; et al. Amplification-free electrochemiluminescence molecular beacon-based microRNA sensing using a mobile phone for detection. *Sens. Actuators, B* **2021**, *330*, 129261.
(28) Sun, J. D.; Sun, X. L. Recent advances in the construction of DNA nanostructure with signal amplification and ratiometric response for miRNA sensing and imaging. *TrAC, Trends Anal. Chem.* **2020**, *127*, 115900.
(29) Wei, T. X.; Du, D.; Wang, Z. Y.; Zhang, W. W.; Lin, Y. H.; Dai, Z. H. Rapid and sensitive detection of microRNA via the capture of fluorescent dyes-loaded albumin nanoparticles around functionalized magnetic beads. *Biosens. Bioelectron.* **2017**, *94*, 56−62.
(30) Chen, F.; Lu, Q. J.; Zhang, Y. Y.; Yao, S. Z. Strand displacement dual amplification miRNAs strategy with FRET between NaYF4:Yb,Tm/Er upconversion nanoparticles and Ti3C2 nanosheets. *Sens. Actuators, B* **2019**, *297*, 126751.
(31) Zhu, D.; Huang, J. X.; Lu, B.; Zhu, Y.; Wei, Y. Q.; Zhang, Q.; Guo, X. X.; Yuwen, L. H.; Su, S.; Chao, J.; et al. Intracellular MicroRNA Imaging with MoS2-Supported Nonenzymatic Catassembly of DNA Hairpins. *ACS Appl. Mater. Interfaces* **2019**, *11*, 20725−20733.
(32) Wang, Y. T.; Wu, N.; Guo, F. N.; Gao, R. X.; Yang, T.; Wang, J. H. g-C3N4 nanosheet-based ratiometric fluorescent probes for the amplification and imaging of miRNA in living cells. *J. Mater. Chem. B* **2019**, *7*, 7566−7573.
(33) Zhou, J.; Li, Z. J.; Ying, M.; Liu, M. X.; Wang, X. M.; Wang, X. Y.; Cao, L. W.; Zhang, H.; Xu, G. X. Black phosphorus nanosheets for rapid microRNA detection. *Nanoscale* **2018**, *10*, 5060−5064.
(34) Bahari, D.; Babamiri, B.; Salimi, A.; Salimizand, H. Ratiometric fluorescence resonance energy transfer aptasensor for highly sensitive and selective detection of Acinetobacter baumannii bacteria in urine sample using carbon dots as optical nanoprobes. *Talanta* **2021**, *221*, 121619.
(35) Zhang, Y.; Ma, C. M.; Ma, C.; Xiang, Y. C.; Mu, S.; Zheng, Z. X.; Liu, X. Y.; Zhang, H. X. Ratiometric fluorescent detection and imaging of microRNA in living cells with manganese dioxide nanosheet-active DNAzyme. *Talanta* **2021**, *233*, 122518.
(36) Qi, Y.; Lu, X. H.; Feng, Q. Y.; Fan, W. J.; Liu, C. H.; Li, Z. P. An Enzyme-Free MicroRNA Assay Based on Fluorescence Counting of Click Chemical Ligation-Illuminated Magnetic Nanoparticles with Total Internal Reflection Fluorescence Microscopy. *ACS Sens.* **2018**, *3*, 2667−2674.
(37) Tang, J.; Liu, L. P.; Qin, J.; Lv, X. T.; Li, J. J.; Tang, D. P.; Zhuang, J. Y. Biocatalysis-mediated MOF-to-prussian blue transformation enabling sensitive detection of NSCLC-associated miRNAs with dual-readout signals. *Biosens. Bioelectron.* **2022**, *206*, 114139.
(38) Han, Z. Y.; Li, S.; Yin, S. X.; Cai, Y. F.; Jin, J.; Huang, G.; Yang, Z. Q. Sensitive and Specific Detecting Biomarker of Radiation-Resistant Nasopharyngeal Carcinoma by TpTta-COF Nanosheet. *Nano* **2021**, *16*, 2150069.
(39) Zhao, Q.; Piao, J. F.; Peng, W. P.; Wang, Y.; Zhang, B.; Gong, X. Q.; Chang, J. Simple and Sensitive Quantification of MicroRNAs via PS@Au Microspheres-Based DNA Probes and DSN-Assisted Signal Amplification Platform. *ACS Appl. Mater. Interfaces* **2018**, *10*, 3324−3332.
(40) Liu, M. Q.; Shen, R.; Li, H. R.; Jia, Y. W.; Mak, P. I.; Martins, R. P. Ratiometric fluorescence analysis for miR-141 detection with hairpin DNA-templated silver nanoclusters. *J. Mater. Chem. C* **2022**, *10*, 655−664.
(41) Ji, D. Y.; Mou, X.; Kwok, C. K. Label-free and ratiometric detection of microRNA based on target-induced catalytic hairpin assembly and two fluorescent dyes. *Anal. Methods* **2019**, *11*, 4808−4813.
(42) Wang, Y. H.; Shao, Z. S.; Cheng, C.; Wang, J. L.; Song, Z.; Song, W. J.; Zheng, F.; Wang, H. S. Fluorescent oligonucleotide indicators for ratiometric microRNA sensing on metal-organic frameworks. *Chem. Eng. J.* **2022**, *437*, 135296.
(43) El Aamri, M.; Yammouri, G.; Mohammadi, H.; Amine, A.; Korri-Youssoufi, H. Electrochemical Biosensors for Detection of MicroRNA as a Cancer Biomarker: Pros and Cons. *Biosensors* **2020**, *10*, 186.
(44) Wang, L. H.; Zeng, H. Q.; Yang, X. L.; Chen, C. M.; Ou, S. Integrated nicking enzyme-powered numerous-legged DNA walker prepared by rolling circle amplification for fluorescence detection of microRNA. *Microchim. Acta* **2021**, *188*, 214.
(45) Liu, L.; Deng, D. H.; Wu, D. H.; Hou, W. L.; Wang, L.; Li, N.; Sun, Z. F. Duplex-specific nuclease-based electrochemical biosensor for the detection of microRNAs by conversion of homogeneous assay into surface-tethered electrochemical analysis. *Anal. Chim. Acta* **2021**, *1149*, 338199.
(46) Ye, J. W.; Xu, M. C.; Tian, X. K.; Cai, S.; Zeng, S. Research advances in the detection of miRNA. *J. Pharm. Anal.* **2019**, *9*, 217−226.
(47) Chen, J.; Xie, M. Y.; Shi, M. Q.; Yuan, K.; Wu, Y. N.; Meng, H. M.; Qu, L. B.; Li, Z. H. Spatial confinement-derived double-accelerated DNA cascade reaction for ultrafast and highly sensitive in situ monitoring of exosomal miRNA and exosome tracing. *Anal. Chem.* **2022**, *94*, 2227−2235.
(48) Shi, M. Q.; Wang, X.; Wu, Y. A.; Yuan, K.; Li, Z. J.; Meng, H. M.; Li, Z. H. Exploring the size of DNA functionalized gold nanoparticles for high efficiency exosome uptake and sensitive biosensing. *Sens. Actuators, B* **2022**, *355*, 131315.
(49) Wu, Y. D.; Cui, S.; Li, Q.; Zhang, R. S.; Song, Z. M.; Gao, Y. Z.; Chen, W. J.; Xing, D. M. Recent advances in duplex-specific nuclease-based signal amplification strategies for microRNA detection. *Biosens. Bioelectron.* **2020**, *165*, 112449.
(50) Yang, J. J.; Zhang, L.; Zhou, Q.; Chen, F.; Stenzel, M.; Gao, F. C.; Liu, C.; Yuan, H. Q.; Li, H.; Jiang, Y. Y. Self-assembled anionic and cationic Au nanoparticles with Au nanoclusters for the exploration of different biological responsiveness in cancer therapy. *Nanoscale Adv.* **2021**, *3*, 2812−2821.
(51) Degliangeli, F.; Kshirsagar, P.; Brunetti, V.; Pompa, P. P.; Fiammengo, R. Absolute and Direct MicroRNA Quantification Using DNA-Gold Nanoparticle Probes. *J. Am. Chem. Soc.* **2014**, *136*, 2264−2267.
(52) Zhou, D. S.; Liu, X. T.; Liu, X. T.; Xu, Y. T.; Chen, R. Q.; Lin, C.; Guo, L. Q.; Fu, F. F. Ratiometric fluorescent biosensor for microRNAs imaging in living cells. *Sens. Actuators, B* **2020**, *322*, 128632.
(53) Wang, S.; Wang, L.; Xu, X. W.; Li, X.; Jiang, W. MnO2 nanosheet-mediated ratiometric fluorescence biosensor for MicroRNA detection and imaging in living cells. *Anal. Chim. Acta* **2019**, *1063*, 152−158.
(54) Wang, Z. .Z.; Xue, Z. Q.; Hao, X. L.; Miao, C. F.; Zhang, J. Z.; Zheng, Y. J.; Zheng, Z. F.; Lin, X. H.; Weng, S. H. Ratiometric fluorescence sensor based on carbon dots as internal reference signal and T7 exonuclease-assisted signal amplification strategy for microRNA-21 detection. *Anal. Chim. Acta* **2020**, *1103*, 212−219.
(55) Zhang, W. Y.; Hao, W. H.; Liu, X. T.; Sun, X. R.; Yan, J. L.; Wang, Y. C. Visual detection of miRNAs using enzyme-free amplification reactions and ratiometric fluorescent probes. *Talanta* **2020**, *219*, 121332.
(56) Zhang, W.; Peng, P.; Kuang, Y.; Yang, J. X.; Cao, D. Y.; You, Y.; Shen, K. Characterization of exosomes derived from ovarian cancer cells and normal ovarian epithelial cells by nanoparticle tracking analysis. *Tumor Biol.* **2016**, *37*, 4213−4221.

https://doi.org/10.1021/acs.bioconjchem.2c00309
Bioconjugate Chem. 2022, 33, 1698−1706